Flow mechanotransduction regulates traction forces, intercellular forces, and adherens junctions

Lucas H. Ting, Jessica R. Jahn, Joon I. Jung, Benjamin R. Shuman, Shirin Feghhi, Sangyoon J. Han, Marita L. Rodriguez and Nathan J. Sniadecki

Am J Physiol Heart Circ Physiol 302:H2220-H2229, 2012. First published 23 March 2012; doi:10.1152/ajpheart.00975.2011

Am J Physiol Heart Circ Physiol 302: H2220–H2229, 2012.
First published March 23, 2012; doi:10.1152/ajpheart.00975.2011.

Flow mechanotransduction regulates traction forces, intercellular forces, and adherens junctions

Lucas H. Ting,[1] Jessica R. Jahn,[2] Joon I. Jung,[1] Benjamin R. Shuman,[1] Shirin Feghhi,[1] Sangyoon J. Han,[1] Marita L. Rodriguez,[1] and Nathan J. Sniadecki[1,3]

[1]*Department of Mechanical Engineering,* [2]*School of Medicine, and* [3]*Department of Bioengineering, University of Washington, Seattle, Washington*

Submitted 11 October 2011; accepted in final form 19 March 2012

Ting LH, Jahn JR, Jung JI, Shuman BR, Feghhi S, Han SJ, Rodriguez ML, Sniadecki NJ. Flow mechanotransduction regulates traction forces, intercellular forces, and adherens junctions. *Am J Physiol Heart Circ Physiol* 302: H2220–H2229, 2012. First published March 23, 2012; doi:10.1152/ajpheart.00975.2011.—Endothelial cells respond to fluid shear stress through mechanotransduction responses that affect their cytoskeleton and cell-cell contacts. Here, endothelial cells were grown as monolayers on arrays of microposts and exposed to laminar or disturbed flow to examine the relationship among traction forces, intercellular forces, and cell-cell junctions. Cells under laminar flow had traction forces that were higher than those under static conditions, whereas cells under disturbed flow had lower traction forces. The response in adhesion junction assembly matched closely with changes in traction forces since adherens junctions were larger in size for laminar flow and smaller for disturbed flow. Treating the cells with calyculin-A to increase myosin phosphorylation and traction forces caused an increase in adherens junction size, whereas Y-27362 cause a decrease in their size. Since tugging forces across cell-cell junctions can promote junctional assembly, we developed a novel approach to measure intercellular forces and found that these forces were higher for laminar flow than for static or disturbed flow. The size of adherens junctions and tight junctions matched closely with intercellular forces for these flow conditions. These results indicate that laminar flow can increase cytoskeletal tension while disturbed flow decreases cytoskeletal tension. Consequently, we found that changes in cytoskeletal tension in response to shear flow conditions can affect intercellular tension, which in turn regulates the assembly of cell-cell junctions.

endothelial cells; microposts; tight junction; shear flow

MECHANOTRANSDUCTION to laminar or disturbed flow in endothelial cells (ECs) can strongly affect their ability to maintain the barrier between blood and the vessel wall (3, 4, 9, 13, 14). Laminar flow occurs in straight vessels and produces a steady shear stress on the cells. Disturbed flow forms downstream of obstructions, bends, or bifurcations and produces a time-averaged low shear stress due to eddies in the flow. It has been proposed that these flows can activate mechanosensors in ECs that lead to the activation of signaling pathways that affect cytoskeletal structures (3, 14). In particular, laminar flow can initiate Rho GTPase pathways, which cause alignment of actin filaments and assembly of adherens junctions (27, 29, 35, 42–46, 49). Conversely, disturbed flow leads to disorganized actin, disassembly of adherens junctions, and small gaps between adjacent ECs (3–5, 27, 30, 31). These structural changes in ECs can strongly affect the integrity of the vascular barrier (7, 17, 31).

It is possible that shear flow affects adherens junction assembly in ECs by influencing their cytoskeletal tension. Laminar flow has been seen to activate RhoA and cause higher traction forces in individual ECs (36, 49). In nonflow conditions, a rise in cytoskeletal tension for a pair of cells in contact with each other not only causes an increase in traction forces but also leads to tugging forces across the cell-cell contact (24, 25). Subsequently, cells within a monolayer have many cell-cell contacts with each other and can impart multiple tugging forces on their neighbors that give rise to intercellular tension, which in turn can affect proliferation and collective migration of the tissue layer (28, 38, 41). How these changes in traction forces and tugging forces affect the barrier function of ECs is not well understood, but it has been seen that forces applied directly at the cell-cell contact can promote the assembly and strengthening of adherens junctions (18, 24, 33, 51). Taken together, shear flow may be an important mechanism that regulates the integrity of the endothelium by modulating cytoskeletal tension and intercellular tension and thereby eliciting a mechanotransduction response at the cell-cell contact that promotes junction assembly.

A rise in traction forces under laminar flow has previously been reported for migrating ECs (36), but the effect of laminar or disturbed flow on the generation of traction forces and intercellular forces for monolayers of ECs is not known. Moreover, this previous study measured traction forces during the first half-hour of shear, a time frame in which several signaling pathways associated with shear flow are activated, as reviewed in Ref. 9, but cytoskeletal structures and traction forces are still in flux (8, 16, 37, 40). A longer study would permit ECs in a monolayer to undergo further rearrangement of their cytoskeletal filaments and cell-cell contacts in response to shear. For these reasons, human pulmonary artery ECs (HPAECs) were cultured as monolayers on arrays of microposts and exposed to static, laminar, and disturbed flow conditions in a custom-built flow chamber for 14 h (Fig. 1). Changes in traction forces, intercellular forces, and cell-cell junctions were measured, and it was found that tension at the cell-cell interface could regulate the barrier function of ECs.

MATERIALS AND METHODS

Cell culture and reagents. HPAECs (Lonza) were thawed and cultured in Ham's F-12 K media (Thermo Scientific), 10% FBS (GIBCO), 1% penicillin (Mediatech), 1% streptomycin (Mediatech), 1% L-glutamine (GIBCO), and supplements from EGM-MV SingleQuot Kits (Lonza). Cells were grown on tissue culture dishes precoated with 1% gelatin (Sigma-Aldrich) from *passages 6* to *8*.

Address for reprint requests and other correspondence: N. Sniadecki, Dept. of Mechanical Engineering, Campus Box 352600, Univ. of Washington, Seattle, WA 98195 (e-mail: nsniadec@uw.edu).

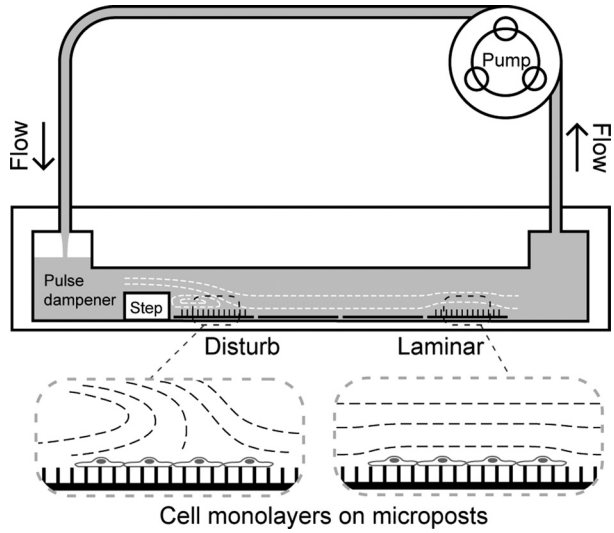

Fig. 1. A custom-built flow chamber with microposts was used to measure traction forces and intercellular forces. Cells cultured on micropost substrates or flat substrates were placed inside a shear flow chamber, and media was circulated across the cells. A backward-facing step in the channel created a zone of recirculation in the media. Cells within this region experienced disturbed flow conditions. Further downstream, the flow stabilized and the cells were subjected to laminar flow.

HPAECs were then seeded at confluent densities onto arrays of biofunctionalized microposts or flat substrates. Cells were allowed to spread and reform their adherens junctions for 2 days in culture before they were subjected to flow conditions for 14 h. DMSO (Tyco) was used to make solutions of Y-27632 (Sigma-Aldrich) and calyculin-A (LC Laboratories).

Preparation of substrates. Flat substrates were created by casting a film of polydimethylsiloxane (PDMS; Dow Corning) with a 0.25 mm thickness on a no. 2 glass coverslip (VWR). Arrays of PDMS microposts were micromolded onto glass coverslips, as previously described (39). To prepare the flat substrates and microposts for cell attachment, fibronectin (50 μg/ml, BD Biosciences) was absorbed onto the surface of a PDMS stamp. The stamps used in this study either had no pattern ("flat stamp") or had an array of positive relief patterns in the shape of 160 × 160-μm squares ("square stamps"). Once the protein was adsorbed, the stamp was placed into conformal contact with the substrate to transfer fibronectin onto the regions of contact. Afterward, each substrate was treated with 0.2% Pluronic F-127 (Sigma-Aldrich) to ensure that the cells adhered to regions where only fibronectin was printed.

Micropost deflection. Microposts act as elastic, cantilever beams that deflect in proportion to the force applied at their tips. To measure the deflection of a micropost, the difference between the position of its tip and base were analyzed from fluorescent images taken at the top and bottom of the arrays, as previously described (21). The magnitude and direction of each traction force (F) was computed from the deflection (δ) through the following relationship:

$$F = \frac{3\pi E D^4}{64 L^3}\delta \qquad (1)$$

The length (L = 6.34 μm) and diameter (D = 2.81 μm) of the microposts in the array were measured using a scanning electron microscope (FEI Sirion SEM). Young's modulus of PDMS (E = 2.5 MPa) was determined by tensile testing, as previously described (23). Microposts in the array had 6-μm center-to-center spacing. Cytoskeletal tension was assessed by computing the average traction force per monolayer. Intercellular forces were determined by the vector sum of the traction forces under a cell in a monolayer (APPENDIX). Intercellular tension was measured by the average intercellular force for cells within a monolayer.

Shear flow chamber. A custom-built parallel plate flow chamber was constructed out of clear acrylic to subject cells to shear flow conditions (Fig. 1). Substrates with HPAEC monolayers were placed inside the chamber, and shear was applied continuously for 14 h. The design of the chamber was intended to be similar to those used previously to produce laminar or disturbed flow on cells, albeit with the addition of arrays of microposts inside the chamber (5, 31). The main channel was 100 mm long, 20 mm wide, and 0.5 mm high. A steady flow rate of 2 ml/s was produced by a peristaltic pump (Control Company), which was connected to the flow chamber and recirculated the media through the chamber. A chamber of air at the entrance of the channel damped the pulsatile flow so that a steady flow rate was produced in the channel. The fluid drag forces on the posts were considered to be negligible (APPENDIX). A 0.25-mm tall, backward-facing step in the channel produced a region of disturbed flow downstream from the step. Flow in this region had separation in its fluid stream lines, a stagnation point, and a region of reversal in the direction of flow. The wall shear stress in the disturbed flow region was estimated to be between −2.4 and 1.9 Pa and had a spatial average of 0.75 Pa, based on a previous study (5). Laminar flow occurred further downstream from the region of disturbed flow and produced a wall shear stress (τ) of 1.7 Pa (17 dyn/cm^2), as given by:

$$\tau = \frac{6\mu Q}{wh^2} \qquad (2)$$

where viscosity ($\mu = 7 \times 10^{-4}$ Pa·s), flow rate (Q), width (w), and height (h) of the channel were determined beforehand. To confirm the location of the laminar and disturbed flow regions, polystyrene beads with a diameter of 19 μm were added to the media to act as flow tracers. Disturbed flow was observed to form over a region downstream from the step that was 4 mm long. Laminar flow was seen to occur further downstream of the disturbed region and was steady along the length of the channel.

Immunofluorescence staining and microscopy. After each experiment, substrates were removed from the flow chamber and fixed with 3.5% paraformaldehyde (Electron Microscopy Supplies). Cells were permeabilized using 0.2% Triton X-100 (Sigma) and then blocked in 10% goat serum (Invitrogen). Primary immunofluorescent staining was conducted using 1:400 mouse IgG anti-β-catenin antibody clone E-5 (Santa Cruz Biotechnology), 1:400 mouse IgG anti-zona occludens (ZO)-1 antibody clone ZO1–1A12 (Invitrogen), or 1:400 rabbit anti-diphospho-myosin light chain 2 polyclonal antibody (Cell Signaling Technology). Secondary staining consisted of 1:200 goat anti-mouse IgG conjugated with Alexa fluor 647 IgG or goat anti-rabbit IgG conjugated with Alexa fluor 647 IgG (Invitrogen), 1:1,000 Hoescht 33342, and 1:500 phalloidin Alexa fluor 488. A Nikon Eclipse Ti inverted microscope with a ×40 or ×60 oil objective and type-DF immersion oil (Cargille) was used for imaging the samples.

Image analysis of actin alignment, phosphorylated myosin, and size of cell-cell junctions. The direction of actin filament alignment was determined using a custom-written code in MATLAB that analyzed the images of phalloidin staining as previously described (15, 52). Briefly, the intensity of each pixel within an image was compared with its neighboring pixels. A vector was then generated, which was directed toward the maximum gradient and had a magnitude corresponding to the gradient. Pixels near an actin filament had vectors with high magnitudes that pointed toward the center of the filament, whereas pixels at a distance from a filament had much lower magnitudes. Vectors that were lower than 40% of the peak magnitude in an image were considered part of the background signal and were not analyzed. The remaining vectors were rotated 90° so that they were aligned parallel to the actin filaments. They were subsequently binned and counted in accordance with their direction to plot their circular distributions as a rose plot.

Phosphorylation levels of myosin for untreated cells and those treated with Y-27642 or calyculin-A were quantified by summing the pixel intensity from images of samples stained with anti-diphospho-myosin light chain antibody, as previously described (2). Briefly, the average fluorescence intensity per pixel was measured for a monolayer of cells. The difference between this value and the background fluorescence was used to determine the amount of diphospho-myosin light chain in cells that were imaged. The background fluorescence level for each sample was measured by determining the average fluorescence intensity per pixel for a region where there were no cells.

Adherens junctions were quantified by analysis of the pixel intensities in images of HPAEC monolayers with immunofluorescently labeled β-catenin. Since immunofluorescence staining can vary from experiment to experiment, each replication of an experiment was stained and imaged as a group with one or more samples from static, laminar, and disturbed flow conditions. All samples within a replication group were imaged using identical shutter dwell times, fluorescent illumination intensity levels, camera gain, camera frequency, and camera binning. A custom-written image analysis code in MATLAB was developed to measure the pixel intensity along the boundaries of the cells (see Fig. 5). To identify the cell boundaries, pixel dilation was first used to join disconnected regions between adherens junction plaques, and the pixels at the boundaries were then isolated from the diffusive cytoplasmic staining by subtracting out the pixels below 30% of the maximum pixel intensity in an image. Next, a watershed algorithm was used to demarcate a line along the cell boundaries. A ribbon of interest was defined by the lines and had a width of 10 pixels. The total intensity of the pixels within the ribbon of interest was calculated and then divided by the total length of the ribbon and the number of cells in the image to determine the amount of junctional β-catenin per length per cell. An identical approach was used to quantify the tight junctions from images of cells stained with ZO-1 antibodies.

Statistical analysis. Samples were analyzed for significance using ANOVA with a Bonferroni's post hoc adjustment. For actin alignment shown in the rose plots, a parametric, two-sample second-order analysis of angles was used to conduct a hypothesis test for cells on flat substrates, whereas a nonparametric, second-order analysis using the Watson's U^2-test was used to conduct a hypothesis test for cells on posts (53). Comparisons were considered significant for P values of <0.05 (marked with asterisks in the figures).

RESULTS

Cytoskeletal tension increases under laminar flow but decreases under disturbed flow. A common response in ECs to shear flow is for their actin filaments to align in the direction of flow. In our flow chamber, we confirmed that HPAECs grown on flat substrates (Fig. 2, *A–C*) align their actin filaments parallel to the direction of laminar flow, whereas under static and disturbed flow, their actin had no preferential alignment (Fig. 2, *D–F*). The angular distribution for actin filaments in cells under laminar flow was statistically different than the distribution under static conditions ($P < 0.05$ by a parametric second-order test), whereas cells under disturbed flow and static conditions had angular distributions that were statistically similar. Likewise, for HPAECs grown on arrays of microposts (Fig. 3, *A–C*), their actin filaments were oriented predominately in the direction of laminar flow but not for static or disturbed flow (Fig. 3, *D–F*). There was, however, a strong degree of actin alignment along the 0, 90, 180, and 270° directions for all flow conditions, which matched the orthogonal arrangement of the microposts in the arrays and the edges of the 160 × 160-μm patterned monolayers (Fig. 3, *D–F*). These results for alignment are reasonable since focal adhesions can form at the microposts and therefore help to confine actin filaments between adjacent posts. Moreover, the edges of the monolayer can cause alignment in actin filaments, as seen previously at a wound edge for ECs (19) or micropatterned lines of cells (22, 47). Despite a degree of orthogonal alignment for micropatterned monolayers on microposts, the angular distribution of actin filaments under laminar flow was statistically different than static conditions ($P < 0.05$ by a second-order Watson U^2-test), whereas the distribution in disturbed flow was statistically similar to static conditions.

Traction forces within a monolayer were measured by analyzing the deflections of the microposts to assess cytoskeletal tension. Vector fields of the traction forces showed that for all flow conditions, traction forces were nonuniform and there were regions of high forces within the monolayers (Fig. 4,

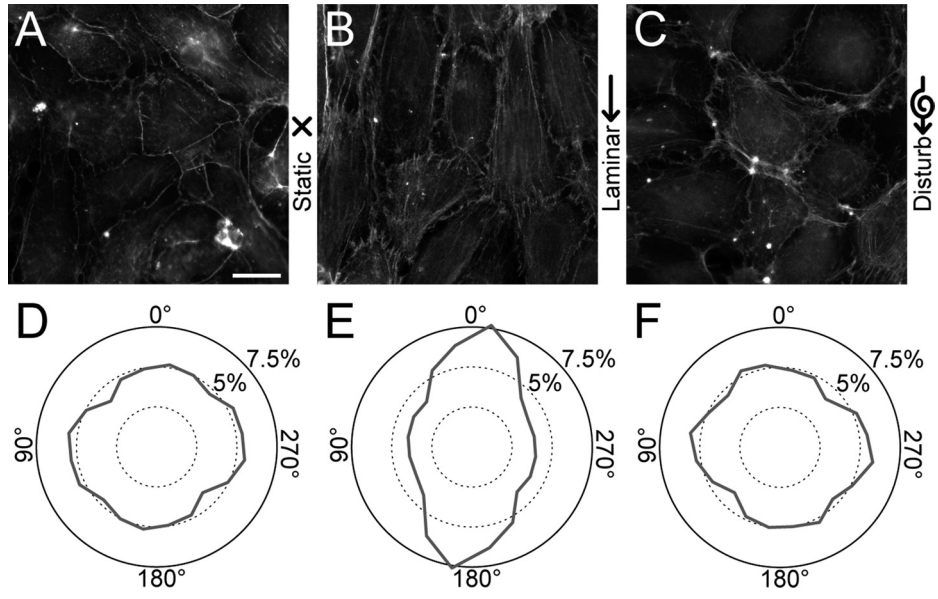

Fig. 2. Endothelial cells (ECs) align their actin filaments in the direction of shear flow on flat substrates. *A–C*: representative immunofluorescent images of actin filaments in human pulmonary artery ECs (HPAECs) cultured on flat substrates and placed under static (*A*), laminar (*B*), or disturbed flow conditions (*C*) for 14 h. *D–F*: rose plots showing the orientations of actin filaments for static (*D*), laminar (*E*), and disturbed flow (*F*). All data collected were from 13 high-power field images/condition and from 3 replicate experiments. Scale bar = 20 μm.

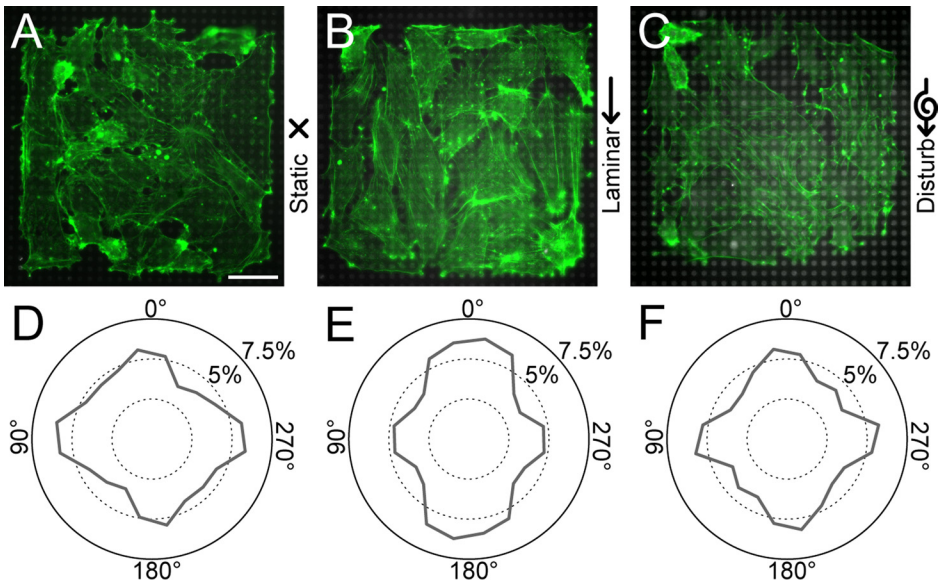

Fig. 3. Actin alignment in endothelial monolayers on microposts depends on flow conditions. *A–C*: representative immunofluorescence images of 160 × 160-μm HPAEC monolayers on microposts after exposure to static (*A*), laminar (*B*), or disturbed flow conditions (*C*) for 14 h (green: actin, gray: microposts). *D–F*: rose plots of actin alignment for static (*D*), laminar (*E*), and disturbed flow conditions (*F*). Actin alignment in the direction of flow was evident for laminar flow conditions. Plots in *D–F* are from 15 samples/condition and from 3 replicate experiments. Scale bar = 40 μm.

A–C). Subjecting HPAECs to laminar flow for 14 h caused their traction forces to be higher on average than static conditions, whereas disturbed flow caused lower traction forces (Fig. 4*D*). The highest traction forces in laminar flow were oriented parallel to the flow, but no alignment was observed for static or disturbed flow (Fig. 4*E*). Thus, these results show that laminar flow affects cytoskeletal tension by aligning actin filaments and traction forces and by producing higher traction forces, whereas disturbed flow does not induce actin or traction force alignment and causes lower traction forces.

Shear stresses affect adherens junction size through cytoskeletal tension. To determine whether cell-cell contacts respond to the modulation in cytoskeletal tension by shear flow, the size of the adherens junctions was quantified using antibodies against β-catenin. This junctional protein binds to vascular endothelial (VE)-cadherin and α-catenin and is essential to the formation of adherens junctions (26, 32). When exposed to laminar flow, β-catenin has been observed to redistribute to the cell boundaries (27, 29). This redistribution occurs predominately without changes in the level of β-catenin expression (27, 35, 46) and has been previously used to characterize the regulation of adherens junction assembly by tugging forces (24).

In our study, HPAEC monolayers were grown on flat substrates, subjected to laminar, disturbed, and static flow conditions as described above, and then stained for β-catenin. HPAECs exposed to laminar flow exhibited adherens junctions that were longer and denser than those for static conditions, whereas disturbed flow had smaller adherens junctions with large gaps between adjacent cells (Fig. 5, *A–C*). A custom image-analysis code was used to determine the size of adherens junctions by identifying the boundaries between cells and then analyzing the pixel intensity of immunofluorescent-labeled β-catenin within the ribbons of interest ("junctional β-catenin"; Fig.

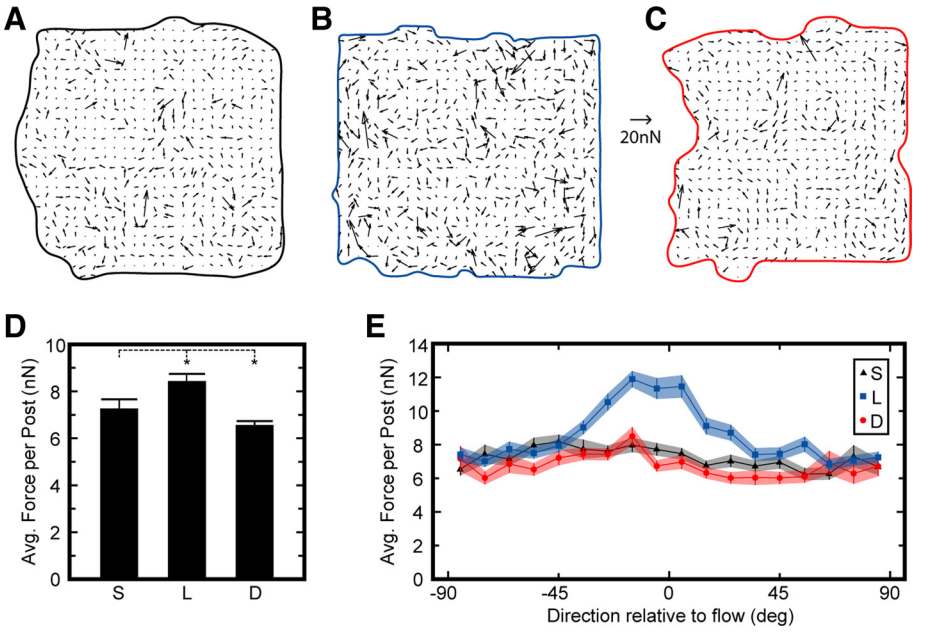

Fig. 4. Shear flow influences the magnitude and direction of traction forces. *A–C*: vector maps of traction forces measured from microposts for representative monolayers. *D*: average traction force per post for monolayers subjected to static (S), laminar (L), and disturbed flow (D) for 14 h. *E*: traction forces oriented in the direction of flow were larger for laminar flow but not for static or disturbed flow. Forces shown in *D* are from 20 monolayers/condition. Data in *E* represent >2,500 posts measured per condition. There were 3 replicate experiments/condition. Force scale bar = 20 nN. $*P < 0.05$.

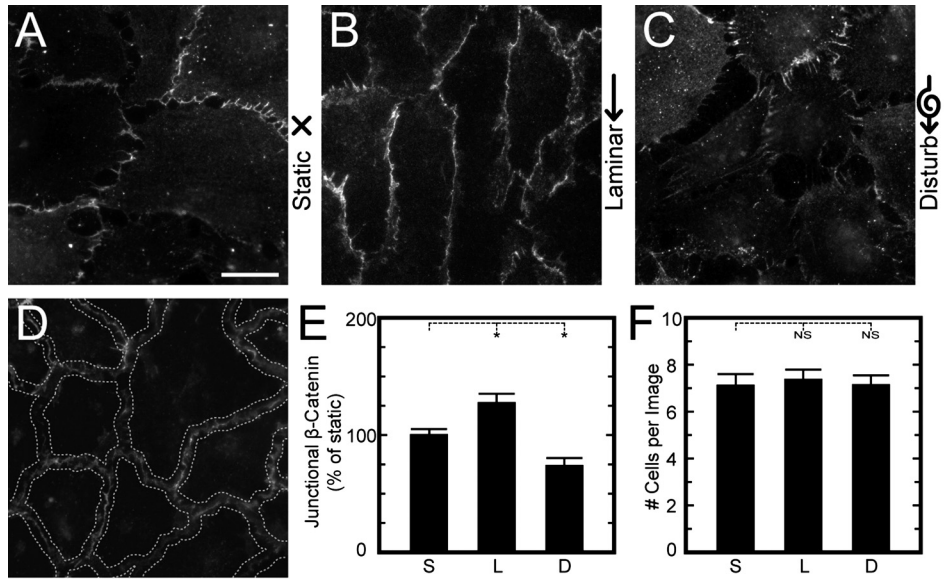

Fig. 5. Analysis of junctional β-catenin was used to assess mechanotransduction at adherens junctions. *A–C*: representative HPAECs on flat substrates were exposed to static (*A*), laminar (*B*), or disturbed flow (*C*) for 14 h and then stained for β-catenin to assess the size of their adherens junctions. *D*: to quantify adherens junction size, a ribbon of interest was created along the border between cells using a watershed algorithm. Fluorescent intensity per unit length along the ribbon of interest was analyzed for each flow condition and divided by the number of cells to measure the amount of junctional β-catenin at the adherens junctions. *E*: compared with static flow conditions, laminar flow increased the amount of junctional β-catenin at the cell-cell contact, whereas disturbed flow decreased adherens junction size. *F*: the number of cells per image did not change with flow condition. Data are from >30 images/condition and from 3 replicate experiments. Scale bar = 20 μm. NS, not significant. $*P < 0.05$.

5*D*). The results for junctional β-catenin were normalized by the results of cells under static conditions for each experiment (Fig. 5*E*). Compared with static conditions, junctional β-catenin was found to be significantly higher for laminar flow and significantly lower for disturbed flow. Changes in junctional β-catenin were not likely due to endothelial turnover caused by proliferation or detachment of cells under shear because the number of cells per high power field was statistically similar for each flow condition (Fig. 5*F*).

To investigate the role of cytoskeletal tension on the regulation of adherens junctions, HPAEC monolayers were treated with 0.3 μM Y-27632 to inhibit Rho kinase (ROCK), a downstream effecter of RhoA that regulates cytoskeletal tension through actin polymerization and myosin phosphorylation. Compared with untreated cells, HPAECs treated with Y-27632 had significantly lower levels of diphospho-myosin light chain (Fig. 6*A*) and lower traction forces (Fig. 6*B*). Higher concentrations of Y-27632 (10 μM) caused a large degree of HPAECs to detach under shear, but at 0.3 μM, HPAECs remained attached and ROCK activity was sufficiently suppressed, as evident by diphospho-myosin levels and traction forces. With Y-27632 treatment, HPAECs had adherens junctions that were significantly reduced in size for laminar and static conditions compared with untreated cells under the same flow conditions (Fig. 6*C*). A reduction in adherens junction size was not observed for cells treated with Y-27632 and under disturbed flow conditions. Thus, these results indicate that inhibition of cytoskeletal tension can reduce the size of adherens junctions to a degree that is similar to cells in disturbed flow.

Conversely, cytoskeletal tension and traction forces were enhanced using calyculin-A, which corresponded with an increase in adherens junction assembly. HPAECs treated with calyculin-A had higher levels of myosin phosphorylation (Fig. 6*A*), which was similar to previous findings for other cell types (2, 12). Treatment with calyculin-A also led to significantly higher traction forces for HPAEC monolayers on the microposts (Fig. 6*B*), which was also similar to previous findings for single cells (20) and paired cells (24). When HPAECs were first subjected to shear flow for 14 h, removed from the flow chamber, and then treated with calyculin-A, the increase in cytoskeletal tension correlated with a significant increase in adherens junction size for cells subjected to laminar or disturbed flow but not for static conditions (Fig. 6*D*). Together,

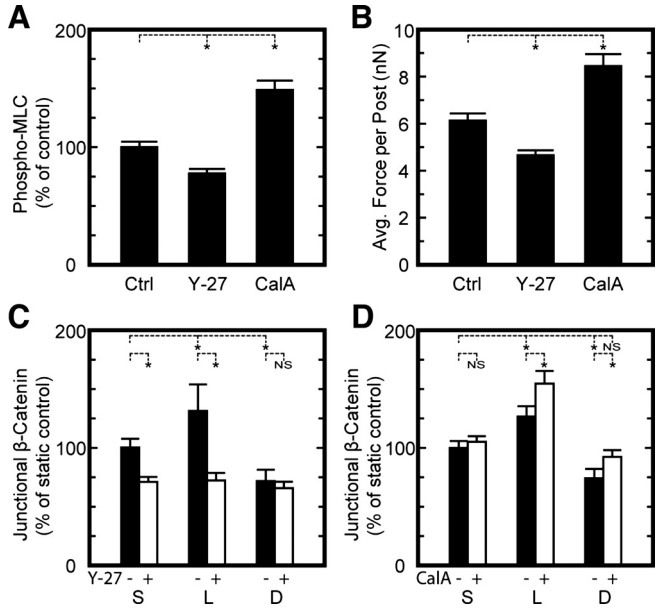

Fig. 6. Cytoskeletal tension can modulate the assembly of adherens junctions under flow. *A*: quantitative microscopy measurements of diphospho-myosin light chain (MLC) levels in HPAEC monolayers on flat substrates in the absence [control (Ctrl)] or presence of 0.3 μM Y-27632 (Y-27) or 2 nM calyculin-A (CalA). Values shown are normalized by results for Ctrl. *B*: traction forces in HPAEC monolayers were lower for Y-27 and higher for CalA. *C*: treatment of HPAECs on flat substrates with Y-27 in the media during 14 h of shear flow reduced the assembly of adherens junction for laminar and static conditions but not for disturbed flow conditions. *E*: exposing HPAECs to shear for 14 h, removing them from the flow chamber, and then treating them with CalA for 10 min caused junctional β-catenin to increase for cells subjected to laminar or disturbed flows but not for static conditions. Data in *A* are from >32 images/condition and from 2 replicate experiments. Data in *B* are from >13 monolayers of cells/condition and from 3 replicate experiments. Data in *C* and *D* are from >28 images/condition and from 3 replicate experiments. $*P < 0.05$.

the results from modulating cytoskeletal tension with Y-27632 and calyculin-A indicate that shear flow affects adherens junction assembly through a mechanotransduction response that involves cytoskeletal tension.

Shear flow affects intercellular tension and adherens junctions. Cytoskeletal tension can be transmitted as traction forces at the microposts but also as intercellular forces between adjacent cells within a monolayer. Tugging forces between paired cells has been previously measured (24, 25), but quantifying all tugging forces within a multicellular structure is mathematically indeterminate. We noted, however, that we could measure the vector sum of the tugging forces, which we defined as the intercellular force acting on a cell (APPENDIX). As before, we grew HPAECs on arrays of microposts and examined the correlation between intercellular forces and adherens junction size. Vector fields of intercellular force showed that cells with large intercellular forces acting on them were located not only at the perimeter but also within the interior of the monolayer (Fig. 7*A*). The average intercellular force was found to be significantly higher for cells subjected to laminar flow compared with those subjected to static and disturbed flow conditions (Fig. 7*B*). Next, the size of adherens junctions for HPAECs on the microposts was analyzed as described above (Fig. 7*C*). We found that junctional β-catenin was high in cells under laminar flow, whereas no difference was observed between cells under static and disturbed flow conditions (Fig. 7*D*).

In addition, shear flow affected the formation of tight junctions in HPAECs. Patterned monolayers were grown on the microposts as described above but were immunofluorescently stained for ZO-1, which marks regions of close contact between plasma membranes of neighboring cells (1). The amount of ZO-1 at the boundaries between cells was analyzed using the same approach as for β-catenin, where the boundaries between cells were identified and ribbons of interests were used to quantify the amount of ZO-1 based on the pixel intensity. The results for each experiment were normalized by the amount of pixel intensity measured for cells under static conditions. Junctional ZO-1 was found to be significantly higher for cells under laminar flow compared with static conditions, whereas it was found to be significantly lower for disturbed flow conditions (Fig. 7*D*). Therefore, these results confirm that shear flow can modulate intercellular tension in a monolayer, which, in turn, affects adherens junction and tight junction size.

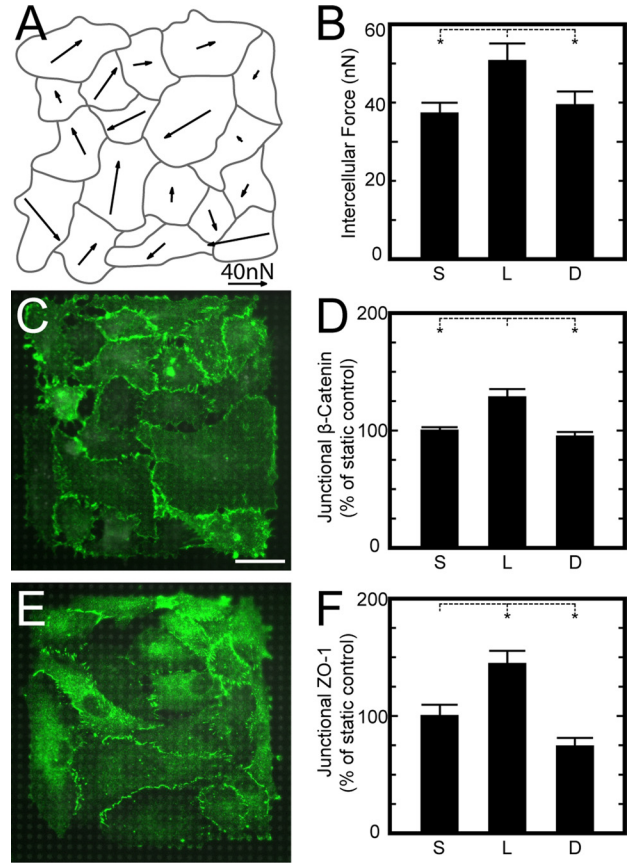

Fig. 7. Intercellular forces increase under laminar flow and promote adherens junction and tight junction assembly. *A*: representative vector map of intercellular forces for an HPAEC monolayer exposed to disturbed flow for 14 h. Intercellular forces were calculated by the vector sum of the tugging forces acting on a cell. *B*: the average intercellular force acting on cells in a monolayer was significantly higher for laminar flow compared with static and disturbed flow. *C*: representative immunofluorescence images of adherens junctions for HPAEC monolayers on microposts under static conditions (green: β-catenin, gray: microposts). *D*: junctional β-catenin at the boundaries between cells in a monolayer was higher for laminar flow but statistically similar for static and disturbed flow. *E*: representative immunofluorescence images of tight junctions for HPAEC monolayers on microposts under static conditions [green: zonula occludens (ZO)-1, gray: microposts]. *F*: junctional ZO-1 at the cell boundaries was higher for laminar flow and lower for disturbed flow. Data in *B* are from >4 monolayers on microposts/condition and taken from 3 replicate experiments. Data in *D* are from >37 monolayers on microposts/condition and taken from 4 replicate experiments. Data in *F* are from >19 monolayers/condition and taken from 2 replicate experiments. $^*P < 0.05$.

DISCUSSION

Using a novel approach of patterned monolayers, microposts, laminar and disturbed flow, and quantitative image analysis, we demonstrated that mechanotransduction of flow conditions directly affects the intercellular tension in a monolayer and that this change coincides with the assembly of cell-cell contacts between adjacent cells. Laminar flow was found to cause a rise in cytoskeletal tension that increased traction forces and intercellular forces and promoted the assembly of adherens junctions and tight junctions. On the other hand, disturbed flow was found to weaken cellular forces and cause adherens junction and tight junction disassembly. Our findings indicate that ECs rely on mechanotransduction in a dual manner: a cell in a monolayer can sense the type of shear flow, align its cytoskeleton, and modulate its traction forces; subsequently, the change in cytoskeletal tension affects the intercellular forces that help to maintain the integrity of its cell-cell contacts.

Traction forces in ECs have been seen to rise when individual cells are subjected to laminar flow (36), but the effect of treating cells to long-term flow conditions has been unclear. A previous study (49) on the activity of RhoA, which can regulate the generation of traction forces, found that RhoA peaks after 5 min of flow, falls back to baseline levels after 15 min, and then rises again to elevated levels for several hours thereafter. However, RhoA has also been observed to decrease after 5 min and stay at reduced levels while under flow (44). Since RhoA regulates stress fiber formation, a reduction in its activity would not likely lead to the increase in actin filaments seen under laminar flow.

Moreover, our observations of high traction forces under laminar flow strongly support that RhoA activity remains elevated after long-term exposure to laminar flow, leading to increased cytoskeletal tension in the monolayer.

On the other hand, the contractile response in ECs to disturbed flow is less clear. Previous studies have found that disturbed flow leads to short actin filaments that are randomly oriented (Ref. 5; for reviews, see Refs. 3 and 4). We found that actin filaments and traction forces are weaker under disturbed flow, which would indicate that RhoA levels are suppressed or that there is an increased inhibition of stress fiber formation. One possibility is that p21-activated kinase (PAK) plays a role in modulating cytoskeletal tension under disturbed flow. PAK activity is elevated in disturbed flow and can, in turn, regulate endothelial permeability (30). PAK is also known to deactivate myosin light chain kinase, which leads to reduced levels of phosphomyosin light chain (34). Although further investigation is required, a correlation between PAK activity, traction forces, and cell-cell junctions could provide an explanation for the changes in endothelial mechanics observed under disturbed flow.

The response in adherens junction to flow has been observed previously (27, 29, 35, 46); however, the mechanisms involved were unexplained. We confirmed the role of cytoskeletal tension on adherens junction assembly by modulating actin-myosin activity with pharmacological inhibitors. Treatment of ECs with Y-27632 caused the size of their adherens junctions to decrease for static and laminar flow but not for disturbed flow conditions. It may be possible to cause further disassembly of adherens junctions with higher concentrations of Y-27632, but we found that this could affect the adhesion strength of cells under flow. Conversely, calyculin-A caused an increase in traction forces and adherens junction assembly, which suggests that cytoskeletal tension is essential to the barrier function of ECs. The increase in adherens junction size was seen for laminar and disturbed flow but not for cells under static conditions. Cells under shear flow have higher levels of Rac1 activity (43, 49), which coregulates the mechanoregulation of adherens junction with tugging forces produced by myosin activity (17). As such, cells under static conditions likely had low levels of Rac1 activity, which undermined the influence of intercellular forces on the assembly of adherens junctions.

It is important to note that endothelial integrity can be compromised by high tension at the cell-cell contacts (6, 11). The results of this study do not disprove this mechanism but instead provide additional evidence that adherens junctions can regulate themselves in proportion to the forces at the cell-cell contact, as others have seen previously (18, 24, 51). To this effect, we quantified changes in adherens junctions by identifying β-catenin localization, which has been shown to colocalize and coimmunoprecipitate with cadherins (6, 50). Since the amount of β-catenin at the border region between cells likely corresponds with an increase in the number of cadherin molecules (6), it is plausible that flow mechanotransduction also affects the adhesion strength between neighboring cells in a monolayer and modulates the structural integrity of the endothelium.

Strong adherens junctions improve the barrier function of ECs by promoting tight junctions that prevent the passage of molecules and ions (10, 26). We also observed a strong similarity between the mechanotransduction response of adherens junctions and tight junctions at the cell-cell junction. The size of both junction types improved under laminar flow and lessened under disturbed flow. Therefore, flow mechanotransduction along different regions of the vasculature can act as another factor that regulates the local permeability of the vessel. For vascular obstructions, however, the disturbance in the flow they cause downstream may also adversely affect intercellular tension in ECs, leading to leaky vessel wells and the rise of atherogenesis.

APPENDIX

Calculation of intercellular forces. In a complex structure such as ECs grown as a monolayer on the microposts, the tugging forces on any given cell are not easily determined. As a consequence, we calculated the intercellular force, which is the vector sum of all of the tugging forces acting on a cell by its neighbors. From this, we were able to assess the intercellular tension within a monolayer by calculating the average intercellular force acting on its cells.

For an isolated cell with no neighbors (Fig. 8A), its tugging force is zero, so its traction forces are in static equilibrium with themselves:

$$\sum_{i}^{n} \vec{\mathbf{F}}_i = 0 \qquad (3)$$

In practice, the vector sum of traction forces ($\mathbf{F}_i$) measured with microposts is generally nonzero but has a very small magnitude (<0.3 nN) and a randomly oriented direction due to measurement errors that are difficult to avoid.

For a pair of cells on microposts (Fig. 8*B*), each cell pulls on the other at the surface of contact between them. Static equilibrium for an individual cell still holds, but the vector sum for its traction forces ($\mathbf{T}_{ij}$) is balanced by the tugging force it produces on its neighbor:

$$\sum_{i}^{n} \vec{\mathbf{F}}_i + \vec{\mathbf{T}}_{ij} = 0 \qquad (4)$$

The tugging force here is opposite in direction to the intercellular force ($\mathbf{I}_i$) acting on the cell (Fig. 8*C*):

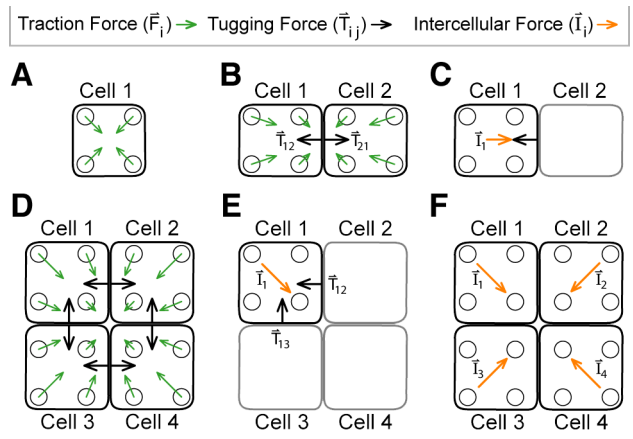

Fig. 8. Calculation of intercellular forces. *A*: an individual cell generates traction forces but not tugging forces. *B*: for pairs of cells, there are tugging forces between them. *C*: the intercellular force experienced by a cell is equal to the vector sum of its tugging forces. *D*: for a monolayer of cells, each cell produces a tugging force on its neighbors, but these forces cannot be solved for uniquely. *E*: as before, the intercellular force on a cell is balanced by the vector sum of its tugging forces. *F*: intercellular forces for cells within a monolayer can be used to assess intercellular tension.

$$\vec{\mathbf{I}}_i = -\vec{\mathbf{T}}_{ij} \quad (5)$$

In this pair-cell system, it is straightforward to calculate the tugging force of a cell and intercellular force acting on it. It only requires measuring one cell's traction forces and calculating the vector sum.

For a group of cells, each tugging force cannot be determined uniquely (Fig. 8*D*). There is static equilibrium for an individual cell within a monolayer, but the vector sum of its traction forces is balanced by its tugging forces, for example:

$$\sum_i^n \vec{\mathbf{F}}_i + \vec{\mathbf{T}}_{12} + \vec{\mathbf{T}}_{13} = 0 \quad (6)$$

The intercellular force acting on a cell can be found as before, by taking the vector sum of the cell's tugging forces (Fig. 8*E*):

$$\vec{\mathbf{I}}_i = -\sum_i^n \vec{\mathbf{T}}_{ij} = -\left(\vec{\mathbf{T}}_{12} + \vec{\mathbf{T}}_{13}\right) \quad (7)$$

Therefore, the intercellular force is equal to the vector sum of the cell's traction forces:

$$\vec{\mathbf{I}}_i = \sum_i^n \vec{\mathbf{F}}_i \quad (8)$$

From this approach, the intercellular tension for monolayer can be assessed by determining the average (Avg) in the magnitude of intercellular forces for N cells within a monolayer (Fig. 8*F*):

$$\text{Avg } I = \frac{1}{N}\sum_j^N \left|\vec{\mathbf{I}}_j\right| = \frac{1}{N}\sum_j^N \left|\sum_i^n \vec{\mathbf{F}}_i\right| \quad (9)$$

Fluid drag on arrays of microposts. Subjecting tall, slender structures like microposts to fluid flow has the potential to cause them to bend from the fluid drag forces acting on them. The configuration of the flow chamber did not allow us to monitor the movement of the posts during the flow experiments, so to investigate the drag forces on the posts, we used analytical and computational approaches. The drag force (F_D) from a fluid of density (ρ) with uniform velocity (v) flowing past a cylinder of length (L) and diameter (D) is given by:

$$F_D = \frac{1}{2} C_D \rho v^2 (LD) \quad (10)$$

where a drag coefficient (C_D) of 90 was approximated for a flow with a Reynold's number of 0.06 (48). The average velocity within the channel was 20 cm/s, but at the region of the microposts, it was determined to be 1.5 cm/s based on Poiseuille flow. Media used in the experiments were assumed to have a similar density as water (993 kg/m^3). Under these conditions, the drag force acting on a single post was determined to be 180 pN, which, in turn, would cause a deflection of ~2 nm. Additionally, a shear stress of 1.7 Pa acting on patterned monolayer of cells (160 × 160 μm) would impart a net force of 44 nN on the monolayer. If this force was distributed across all of the 676 posts underneath a monolayer, it would impart an average force of 65 pN/post, which is smaller than the previous estimate for the fluid drag force on a single post. Furthermore, computation fluid dynamics simulations were run in COMSOL to investigate the drag force on an array of microposts (Fig. 9*A*). The lateral surfaces were defined as slip boundaries to create a uniform flow field in the transverse direction so that a small subset of columns needed to be included in the model. Each array has 1,625 rows and 1,360 columns of microposts, but the array ran in the simulation had significantly fewer posts to reduce the computational time, but without sacrificing the accuracy of the results. From the results of the simulations, posts at the leading edge of the array had the highest deflections of 2.4 nm, which corresponded to a drag force of 220 pN (Fig. 9*B*). For posts within the interior of the array, the reduced velocity of the flow between the posts resulted in an average deflection of 1.3 nm, which equated to a drag force of 0.12 nN. Simulations were run for twice the number of rows of posts, and the results were found to be congruent with the original simulation. Since these deflections were determined to be in the nanometer range and below the measurement resolution of our micropost approach, the effect of fluid drag forces on the posts was considered negligible in our study. Moreover, the deflections of the microposts were measured from samples that were fixed, stained, and mounted on a glass slide, so fluid drag forces were no longer acting on the microposts and can be neglected in our measurements.

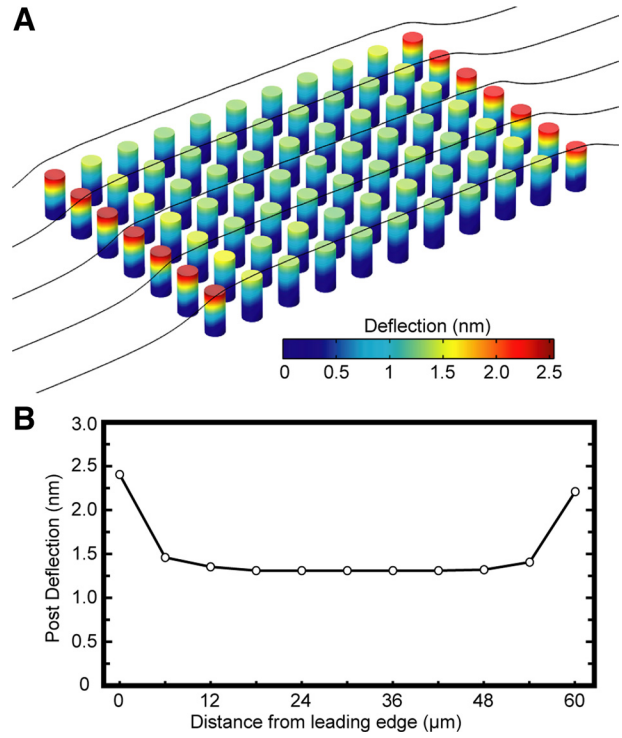

Fig. 9. Shear flow causes negligible drag forces on arrays of microposts. *A*: a computational fluid dynamics model was run in COMSOL to assess the fluid drag forces on an array of microposts. *B*: simulations of the drag force showed that the first and last rows of posts had the largest deflections, but were <2.5 nm. Out of caution, traction force measurements were not taken for monolayers of cells that were positioned close to the edges of the arrays, to avoid any differences in the deflections of the microposts.

ACKNOWLEDGMENTS

The authors thank Alberto Aliseda and Randal Ching for providing helpful discussions on this work.

GRANTS

This work supported in part by National Institutes of Health Grants HL-097284 and EB-001650, a National Science Foundation CAREER award, and University of Washington's Medical Student Research Training Program and Royalty Research Fund.

DISCLOSURES

No conflicts of interest, financial or otherwise, are declared by the author(s).

AUTHOR CONTRIBUTIONS

Author contributions: L.H.T. and N.J.S. conception and design of research; L.H.T., J.R.J., J.I.J., and B.R.S. performed experiments; L.H.T., J.R.J., J.I.J., B.R.S., S.F., S.J.H., and M.L.R. analyzed data; L.H.T., J.R.J., and N.J.S.

interpreted results of experiments; L.H.T. prepared figures; L.H.T. and N.J.S. drafted manuscript; L.H.T. and N.J.S. edited and revised manuscript; L.H.T. and N.J.S. approved final version of manuscript.

REFERENCES

1. **Balda MS, Matter K.** Tight junctions at a glance. *J Cell Sci* 121: 3677–3682, 2008.
2. **Bhadriraju K, Elliott JT, Nguyen M, Plant AL.** Quantifying myosin light chain phosphorylation in single adherent cells with automated fluorescence microscopy. *BMC Cell Biol* 8: 43, 2007.
3. **Chien S.** Effects of disturbed flow on endothelial cells. *Ann Biomed Eng* 36: 554–562, 2008.
4. **Chiu JJ, Chien S.** Effects of disturbed flow on vascular endothelium: pathophysiological basis and clinical perspectives. *Physiol Rev* 91: 327–387, 2011.
5. **Chiu JJ, Wang DL, Chien S, Skalak R, Usami S.** Effects of disturbed flow on endothelial cells. *J Biomech Eng* 120: 2–8, 1998.
6. **Chu YS, Thomas WA, Eder O, Pincet F, Perez E, Thiery JP, Dufour S.** Force measurements in E-cadherin-mediated cell doublets reveal rapid adhesion strengthened by actin cytoskeleton remodeling through Rac and Cdc42. *J Cell Biol* 167: 1183–1194, 2004.
7. **Dai G, Kaazempur-Mofrad MR, Natarajan S, Zhang Y, Vaughn S, Blackman BR, Kamm RD, Garcia-Cardena G, Gimbrone MA Jr.** Distinct endothelial phenotypes evoked by arterial waveforms derived from atherosclerosis-susceptible and -resistant regions of human vasculature. *Proc Natl Acad Sci USA* 101: 14871–14876, 2004.
8. **Dangaria JH, Butler PJ.** Macrorheology and adaptive microrheology of endothelial cells subjected to fluid shear stress. *Am J Physiol Cell Physiol* 293: C1568–C1575, 2007.
9. **Davies PF.** Flow-mediated endothelial mechanotransduction. *Physiol Rev* 75: 519–560, 1995.
10. **Dejana E.** Endothelial cell-cell junctions: happy together. *Nat Rev Mol Cell Biol* 5: 261–270, 2004.
11. **Dudek SM, Garcia JG.** Cytoskeletal regulation of pulmonary vascular permeability. *J Appl Physiol* 91: 1487–1500, 2001.
12. **Fabian L, Troscianczuk J, Forer A.** Calyculin A, an enhancer of myosin, speeds up anaphase chromosome movement. *Cell Chromosome* 6: 1, 2007.
13. **Gimbrone MA.** The Gordon Wilson lecture: Understanding vascular endothelium: a pilgrim's progress: endothelial dysfunction, biomechanical forces and the pathobiology of atherosclerosis. *Trans Am Clin Climatol Assoc* 121: 115–127, 2010.
14. **Hahn C, Schwartz MA.** Mechanotransduction in vascular physiology and atherogenesis. *Nat Rev Mol Cell Biol* 10: 53–62, 2009.
15. **Kaunas R, Nguyen P, Usami S, Chien S.** Cooperative effects of Rho and mechanical stretch on stress fiber organization. *Proc Natl Acad Sci USA* 102: 15895–15900, 2005.
16. **Krishnan R, Park CY, Lin YC, Mead J, Jaspers RT, Trepat X, Lenormand G, Tambe D, Smolensky AV, Knoll AH, Butler JP, Fredberg JJ.** Reinforcement versus fluidization in cytoskeletal mechanoresponsiveness. *PLos One* 4: e5486, 2009.
17. **Langille BL.** Morphologic responses of endothelium to shear stress: reorganization of the adherens junction. *Microcirculation* 8: 195–206, 2001.
18. **le Duc Q, Shi Q, Blonk I, Sonnenberg A, Wang N, Leckband D, de Rooij J.** Vinculin potentiates E-cadherin mechanosensing and is recruited to actin-anchored sites within adherens junctions in a myosin II-dependent manner. *J Cell Biol* 189: 1107–1115, 2010.
19. **Lee JS, Gotlieb AI.** Microtubules regulate aortic endothelial cell actin microfilament reorganization in intact and repairing monolayers. *Histol Histopathol* 20: 455–465, 2005.
20. **Lemmon CA, Chen CS, Romer LH.** Cell traction forces direct fibronectin matrix assembly. *Biophys J* 96: 729–738, 2009.
21. **Lemmon CA, Sniadecki NJ, Ruiz SA, Tan JL, Romer LH, Chen CS.** Shear force at the cell-matrix interface: enhanced analysis for microfabricated post array detectors. *Mech Chem Biosyst* 2: 1–16, 2005.
22. **Li S, Bhatia S, Hu YL, Shiu YT, Li YS, Usami S, Chien S.** Effects of morphological patterning on endothelial cell migration. *Biorheology* 38: 101–108, 2001.
23. **Liang XM, Han SJ, Reems JA, Gao D, Sniadecki NJ.** Platelet retraction force measurements using flexible post force sensors. *Lab Chip* 10: 991–998, 2010.
24. **Liu Z, Tan JL, Cohen DM, Yang MT, Sniadecki NJ, Ruiz SA, Nelson CM, Chen CS.** Mechanical tugging force regulates the size of cell-cell junctions. *Proc Natl Acad Sci USA* 107: 9944–9949, 2010.
25. **Maruthamuthu V, Sabass B, Schwarz US, Gardel ML.** Cell-ECM traction force modulates endogenous tension at cell-cell contacts. *Proc Natl Acad Sci USA* 108: 4708–4713, 2011.
26. **Mehta D, Malik AB.** Signaling mechanisms regulating endothelial permeability. *Physiol Rev* 86: 279–367, 2006.
27. **Miao H, Hu YL, Shiu YT, Yuan S, Zhao Y, Kaunas R, Wang Y, Jin G, Usami S, Chien S.** Effects of flow patterns on the localization and expression of VE-cadherin at vascular endothelial cell junctions: in vivo and in vitro investigations. *J Vasc Res* 42: 77–89, 2005.
28. **Nelson CM, Jean RP, Tan JL, Liu WF, Sniadecki NJ, Spector AA, Chen CS.** Emergent patterns of growth controlled by multicellular form and mechanics. *Proc Natl Acad Sci USA* 102: 11594–11599, 2005.
29. **Noria S, Cowan DB, Gotlieb AI, Langille BL.** Transient and steady-state effects of shear stress on endothelial cell adherens junctions. *Circ Res* 85: 504–514, 1999.
30. **Orr AW, Stockton R, Simmers MB, Sanders JM, Sarembock IJ, Blackman BR, Schwartz MA.** Matrix-specific p21-activated kinase activation regulates vascular permeability in atherogenesis. *J Cell Biol* 176: 719–727, 2007.
31. **Phelps JE, DePaola N.** Spatial variations in endothelial barrier function in disturbed flows in vitro. *Am J Physiol Heart Circ Physiol* 278: H469–H476, 2000.
32. **Pokutta S, Weis WI.** Structure and mechanism of cadherins and catenins in cell-cell contacts. *Annu Rev Cell Dev Biol* 23: 237–261, 2007.
33. **Potard US, Butler JP, Wang N.** Cytoskeletal mechanics in confluent epithelial cells probed through integrins and E-cadherins. *Am J Physiol Cell Physiol* 272: C1654–C1663, 1997.
34. **Sanders LC, Matsumura F, Bokoch GM, de Lanerolle P.** Inhibition of myosin light chain kinase by p21-activated kinase. *Science* 283: 2083–2085, 1999.
35. **Shay-Salit A, Shushy M, Wolfovitz E, Yahav H, Breviario F, Dejana E, Resnick N.** VEGF receptor 2 and the adherens junction as a mechanical transducer in vascular endothelial cells. *Proc Natl Acad Sci USA* 99: 9462–9467, 2002.
36. **Shiu YT, Li S, Marganski WA, Usami S, Schwartz MA, Wang YL, Dembo M, Chien S.** Rho mediates the shear-enhancement of endothelial cell migration and traction force generation. *Biophys J* 86: 2558–2565, 2004.
37. **Sniadecki NJ, Anguelouch A, Yang MT, Lamb CM, Liu Z, Kirschner SB, Liu Y, Reich DH, Chen CS.** Magnetic microposts as an approach to apply forces to living cells. *Proc Natl Acad Sci USA* 104: 14553–14558, 2007.
38. **Tambe DT, Hardin CC, Angelini TE, Rajendran K, Park CY, Serra-Picamal X, Zhou EHH, Zaman MH, Butler JP, Weitz DA, Fredberg JJ, Trepat X.** Collective cell guidance by cooperative intercellular forces. *Nat Mater* 10: 469–475, 2011.
39. **Tan JL, Tien J, Pirone DM, Gray DS, Bhadriraju K, Chen CS.** Cells lying on a bed of microneedles: an approach to isolate mechanical force. *Proc Natl Acad Sci USA* 100: 1484–1489, 2003.
40. **Trepat X, Deng L, An SS, Navajas D, Tschumperlin DJ, Gerthoffer WT, Butler JP, Fredberg JJ.** Universal physical responses to stretch in the living cell. *Nature* 447: 592–595, 2007.
41. **Trepat X, Wasserman MR, Angelini TE, Millet E, Weitz DA, Butler JP, Fredberg JJ.** Physical forces during collective cell migration. *Nat Phys* 5: 426–430, 2009.
42. **Tzima E.** Role of small GTPases in endothelial cytoskeletal dynamics and the shear stress response. *Circ Res* 98: 176–185, 2006.
43. **Tzima E, Del Pozo MA, Kiosses WB, Mohamed SA, Li S, Chien S, Schwartz MA.** Activation of Rac1 by shear stress in endothelial cells mediates both cytoskeletal reorganization and effects on gene expression. *EMBO J* 21: 6791–6800, 2002.
44. **Tzima E, del Pozo MA, Shattil SJ, Chien S, Schwartz MA.** Activation of integrins in endothelial cells by fluid shear stress mediates Rho-dependent cytoskeletal alignment. *EMBO J* 20: 4639–4647, 2001.
45. **Tzima E, Kiosses WB, del Pozo MA, Schwartz MA.** Localized cdc42 activation, detected using a novel assay, mediates microtubule organizing center positioning in endothelial cells in response to fluid shear stress. *J Biol Chem* 278: 31020–31023, 2003.
46. **Ukropec JA, Hollinger MK, Woolkalis MJ.** Regulation of VE-cadherin linkage to the cytoskeleton in endothelial cells exposed to fluid shear stress. *Exp Cell Res* 273: 240–247, 2002.
47. **Vartanian KB, Kirkpatrick SJ, Hanson SR, Hinds MT.** Endothelial cell cytoskeletal alignment independent of fluid shear stress on micropatterned surfaces. *Biochem Biophys Res Commun* 371: 787–792, 2008.

48. **White FM.** *Viscous Fluid Flow*. New York, NY: McGraw-Hill Higher Education, 2006.
49. **Wojciak-Stothard B, Ridley AJ.** Shear stress-induced endothelial cell polarization is mediated by Rho and Rac but not Cdc42 or PI 3-kinases. *J Cell Biol* 161: 429–439, 2003.
50. **Yamada S, Pokutta S, Drees F, Weis WI, Nelson WJ.** Deconstructing the cadherin-catenin-actin complex. *Cell* 123: 889–901, 2005.
51. **Yonemura S, Wada Y, Watanabe T, Nagafuchi A, Shibata M.** α-Catenin as a tension transducer that induces adherens junction development. *Nat Cell Biol* 12: 533–542, 2010.
52. **Yoshigi M, Clark EB, Yost HJ.** Quantification of stretch-induced cytoskeletal remodeling in vascular endothelial cells by image processing. *Cytometry A* 55: 109–118, 2003.
53. **Zar JH.** *Biostatistical Analysis.* Upper Saddle River, NJ: Prentice Hall, 1999.